ELSEVIER

Materials Science and Engineering A 460–461 (2007) 357–364

MATERIALS SCIENCE & ENGINEERING A

www.elsevier.com/locate/msea

Processing and mechanical properties of SiC reinforced cast magnesium matrix composites by stir casting process

Palash Poddar, V.C. Srivastava, P.K. De, K.L. Sahoo *

National Metallurgical Laboratory, Jamshedpur 831007, India

Received 19 July 2006; received in revised form 16 January 2007; accepted 18 January 2007

Abstract

Elemental Mg and Mg-alloy (AZ91D) based composites reinforced with 15 vol.% silicon carbide (SiC) particulates (average particle size 15 μm and 150 μm) were synthesised by stir casting technique. Particle distribution, particle–matrix interfacial reaction, hardness and mechanical properties in the as cast as well as T4 heat-treated conditions were investigated. The composite materials show uniform distribution of SiC particulates. The average grain size decreases with the presence of SiC particulates and the grain size further decreases as the particle size decreases. The AZ91D alloy composite shows an increase in hardness and elastic modulus compared to monolithic alloys. The improvement in elastic modulus of composite containing 15 μm size SiC particles is significantly higher than the composite with 150 μm size particles. The ultimate tensile strength and ductility of composite materials were reduced compared to unreinforced alloy.
© 2007 Elsevier B.V. All rights reserved.

Keywords: Metal matrix composites; Magnesium alloys; Stir casting; SiC particle; Mechanical properties

1. Introduction

The ever-increasing fuel price has led to a renewed urgency to address the issue of weight reduction in the aerospace and automotive sectors. Since magnesium and its alloys are the lightest structural metallic materials having highest specific strength, magnesium based metal matrix composites (MMCs) have attracted considerable interest because of their attractive mechanical properties over monolithic alloy [1]. This is due to the fact that monolithic alloys possess low elastic modulus. This limitation can be circumvented by incorporation of harder and stiffer ceramic particulates in the matrix. However, the selection of the type, size and volume fraction of the reinforcements used are essential to realise optimum properties of these composite materials. Elemental Mg or Mg-alloy matrix composites maintain a low density, high specific strength and stiffness at room temperature as well as elevated temperatures, with a superior wear resistance and damping capacity [2–6]. Therefore, the Mg–matrix composites have been considered as an attractive choice for high performance structural applications in the aerospace and automotive sectors [7,8].

At present, particulate reinforced composites are being produced by different methods, such as stir casting [2–5,9–13], powder metallurgy [14,15], and spray deposition technique [16]. Among these methods, stir casting is considered to be easily adaptable and economically viable due to its low processing cost and high production rate. An additional benefit of this process is the near-net shape formation of the composites. In comparison with Al–matrix composites, the research on Mg–matrix composites are still limited. The key reason is perhaps related to the difficulty in synthesising Mg–matrix composites due to the high chemical activity of Mg. In general, flux and/or protective atmosphere are used to avoid burning of magnesium melt. A number of reports [2,4,9–13] are available on Mg-alloys + SiC composites, the effects of SiC particle size on the microstructure and mechanical properties are meagre. Therefore, the objective of the present study is to develop a stir casting process to produce SiC reinforced cast Mg and Mg-alloy matrix composites, and to investigate their microstructure and mechanical properties. The microstructure and mechanical properties of the as cast and T4 heat-treated composite materials are compared with unreinforced materials.

* Corresponding author. Tel.: +91 657 2271709; fax: +91 657 2270527.
E-mail address: klsah@nmlindia.org (K.L. Sahoo).

0921-5093/$ – see front matter © 2007 Elsevier B.V. All rights reserved.
doi:10.1016/j.msea.2007.01.052

Table 1
Nominal chemical compositions of elemental matrix Mg and Mg-alloys in weight percent

Alloy	Al	Zn	Si	Mn	Fe	Cu	Ni	Mg
Elemental-Mg	0.106	0.043	0.001	0.013	0.018	0.024	0.001	Rest
AZ91D	9.0	0.81	0.1	0.24	0.022	0.030	0.005	Rest

2. Experimental method

2.1. Composite casting

Commercially available elemental Mg (99.8% purity) and AZ91D alloy were processed, and their nominal chemical compositions are given in Table 1. The processing of AZ91D alloy was carried out by melting Mg ingot pieces in a mild steel crucible, kept in a resistance furnace, under the cover of a flux (20% KCl, 50% $MgCl_2$, 15% MgO, 15% CaF_2, wt.%) and high purity (99.98%) argon gas. In order to compensate the oxidation losses, 10 wt.% Mg, 5 wt.% Al and 10 wt.% Zn were taken in excess to the required amount of these constituents. Manganese was incorporated in the melt using anhydrous $MnCl_2$. Elemental Mg ingots were also melted following the identical processing conditions. Magnesium matrix composites reinforced with 15 vol.% α-SiC (15 μm and 150 μm average size) were produced by the stir casting process. The processing of materials and their designation are summarised in Table 2.

A charge of 2 kg of AZ91D (A2) alloy was placed in a mild steel crucible preheated to 400 °C, in an electric resistance furnace along with 1.0 wt.% preheated cover flux, mentioned earlier. Thereafter, argon gas was allowed to pass to avoid burning of Mg during melting. The furnace temperature was raised to 680 °C and the melt was homogenised for about 30 min. Then the melt temperature was further increased to 700 °C. Preheated flux was added and the melt was homogenised for 8–10 min by stirring up and down with a skim ladle. The melt temperature was brought down to around 680 °C. After cleaning the surface of the melt, preheated (up to 250 °C) SiC particles were added into the vortex of the melt during stirring. The composite melt was stirred with stainless steel impeller at 650 rpm for 20 min. The composite melt temperature was around 620–630 °C at the end of the stirring process. It was then heated rapidly to about 700 °C and poured into a permanent steel mould to form ingot of 150 mm × 80 mm × 20 mm size. Similar ingots were also produced for pure Mg-composite. The ingots of the composites and unreinforced Mg-alloy were subjected to a solution heat treatment (T4) for 18 h at 415 °C under a protective atmosphere of CO_2.

Table 2
Materials designation and processing condition

Material	Condition	Particle size (μm)	Designation
Mg	As-cast	–	A1
AZ91D	As-cast	–	A2
AZ91D	T4	–	A3
Mg/15 SiCp	As-cast	150	C1
AZ91D/15 SiCp	As-cast	150	C2
AZ91D/15 SiCp	As-cast	15	C3
AZ91D/15 SiCp	T4	150	C4
AZ91D/15 SiCp	T4	15	C5

2.2. Porosity and particulate content measurement

Quantitative analysis of incorporated SiC particulates in the composites was carried out using the chemical dissolution method, the detail of which is given elsewhere [17,18]. Five samples were taken for each category of specimen and average weight fraction was determined. In this calculation, density of SiC (ρ_p) was taken to be 3.2 g cm^{-3}. The densities of matrix alloy as well as composites were measured, using the Archimedes' principle, to quantify the volume fraction of porosity. Porosity of the composites was estimated using the following relation:

$$\text{porosity}\,(P) = 1 - \frac{\rho_{mc}}{\rho_m(1 - V_p) + \rho_p V_p}$$

where ρ_{mc} is the measured density of the composites, ρ_m is the theoretical density of the matrix alloy and V_p is the volume fraction of SiC.

2.3. Microstructural characterisation

Microstructural characterisation was carried out for both etched and unetched samples under an optical microscope attached with an image analyser. Acetic picral (4.2 g picric acid, 10 ml acetic acid, 10 ml distilled water, 70 ml of 95% ethyl alcohol) was used as etching reagent for all the samples. The average grain size, morphological characteristics of second phase and distribution of SiC particulates were evaluated. The grain-size measurement was also performed on the solution heat-treated specimens according to ASTM standard E 112-96. At least ten fields were randomly chosen for each specimen to ensure an uncertainty less than 5%. The matrix/particle interfacial integrity was examined using a scanning electron microscope (SEM) coupled with energy dispersive spectroscopy (EDS). X-ray diffraction studies (Cu Kα, λ = 1.5418 Å) were carried out on as cast A2 alloy and C2 composite at a scanning speed of 2° min^{-1}.

2.4. Property evaluation

Mechanical properties of as cast and T4 heat-treated specimens were evaluated in terms of their microhardness, macrohardness and tensile properties. Microhardness measurements were carried out to evaluate the effect of the addition of SiC particulates and their size on the hardness of the matrix as well as the Mg/SiC interface using an automatic digital microhardness tester at a load of 50 g. The macrohardness mea-

Table 3
Characterisation results obtained from pure Mg and its alloys and composites

Material	Theoretical density (g cm^{-3})	Experimental density (g cm^{-3})	SiC content (wt.%)	SiC (vol.%)	Porosity (vol.%)	Grain size (μm)
A1	1.740	1.738	–	–	0.11	172.8 ± 2
A2	1.810	1.807	–	–	0.14	–
A3	–	–	–	–	–	166.7 ± 3
C1	1.960	1.934	24	15.1	1.33	76.6 ± 3
C2	2.018	1.990	23.7	15	1.37	–
C3	2.015	1.986	23.4	14.8	1.44	–
C4	–	–	–	–	–	84.3 ± 2
C5	–	–	–	–	–	68.4 ± 2

surements were carried out on Vickers macrohardness tester, at a load of 2.5 kg. The tensile samples were fabricated following ASTM E8M-03 subsize flat specimen standard (25 mm in gauge length, 6 mm in width and 5 mm in thickness). The tensile tests were carried out on an INSTRON testing machine at a strain rate of 1×10^{-4} s^{-1}. Fracture surfaces were studied under SEM to find out the fracture mechanism.

3. Results

Table 3 shows the variation of porosity and SiC content in the cast materials. This indicates that the density of both the unreinforced alloy and composites are close to their theoretical density. However, the composites invariably show larger amount of porosity compared to monolithic materials. A low porosity fraction of composite indicates the efficiency of the processing technique to produce good ingots. Chemical dissolution test result shows that SiC volume fraction is close to the intended amount in pure Mg as well as Mg-alloy matrices.

The microstructural examination of the cast alloy (A2) revealed a two-phase microstructure (Fig. 1). This depicts indistinguishable eutectic-α and primary α-phases, and the another constituent of eutectic equilibrium β-precipitates ($Mg_{17}Al_{12}$) along the grain boundaries and also adjacent to the grain boundary. It also reveals that the β-phase does not envelop the grain boundary completely. The composition of β-phase was detected by EDS analysis and complemented by XRD analysis (Fig. 2). There was no detectable trace of phases related to Si–O and Mg–O systems in the samples indicating absence of oxide products. SEM study of composite sample shows fairly uniform distribution of SiC particles in pure Mg and Mg-alloy matrix (Figs. 3 and 4). The C1 and C2 composite samples show better distribution of SiC particles when compared with C3 composite sample, which shows agglomeration of SiC particles in some areas. The interfacial integrity of SiC particulates with the matrix is found to be good in all samples characterised (Fig. 4c). Interfacial integrity here is defined as good bonding and no traces of interfacial reaction product. This has been confirmed by XRD and SEM. A sharp and clean interface (i.e. precipitate and reaction free) indicates no reaction at the interface.

This conclusion is based on the fact that no detectable interfacial products were observed and no residual pore forms at the interface. The composite specimens exhibit relatively finer grain sizes compared with the unreinforced samples (Table 3). The composite C1 shows 56% decrease in average grain size when compared with 173 μm for pure Mg (A1). Similarly, 48%

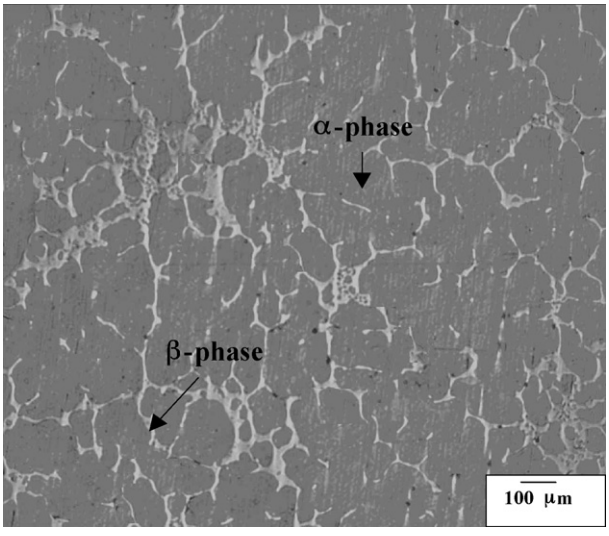

Fig. 1. Micrographs of A2 alloy showing distribution of precipitate phase at the grain boundaries.

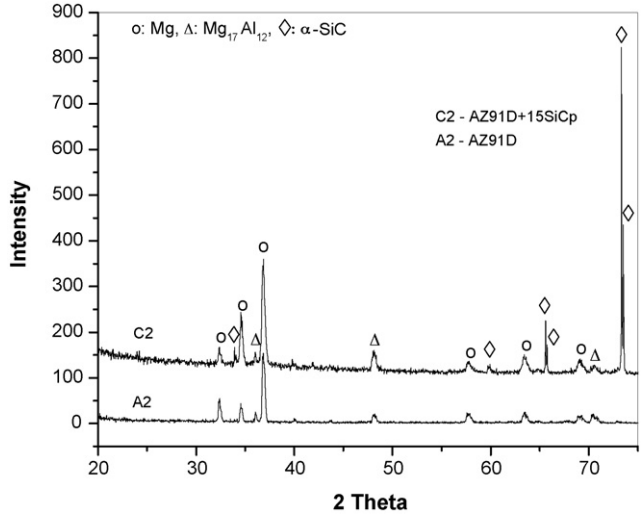

Fig. 2. XRD patterns of A2 alloy and C2 composite obtained at identical processing conditions. The A2 alloy shows peaks of Mg and $Mg_{17}Al_{12}$-phase whereas C2 composite shows the peaks of Mg, $Mg_{17}Al_{12}$ and α-SiC.

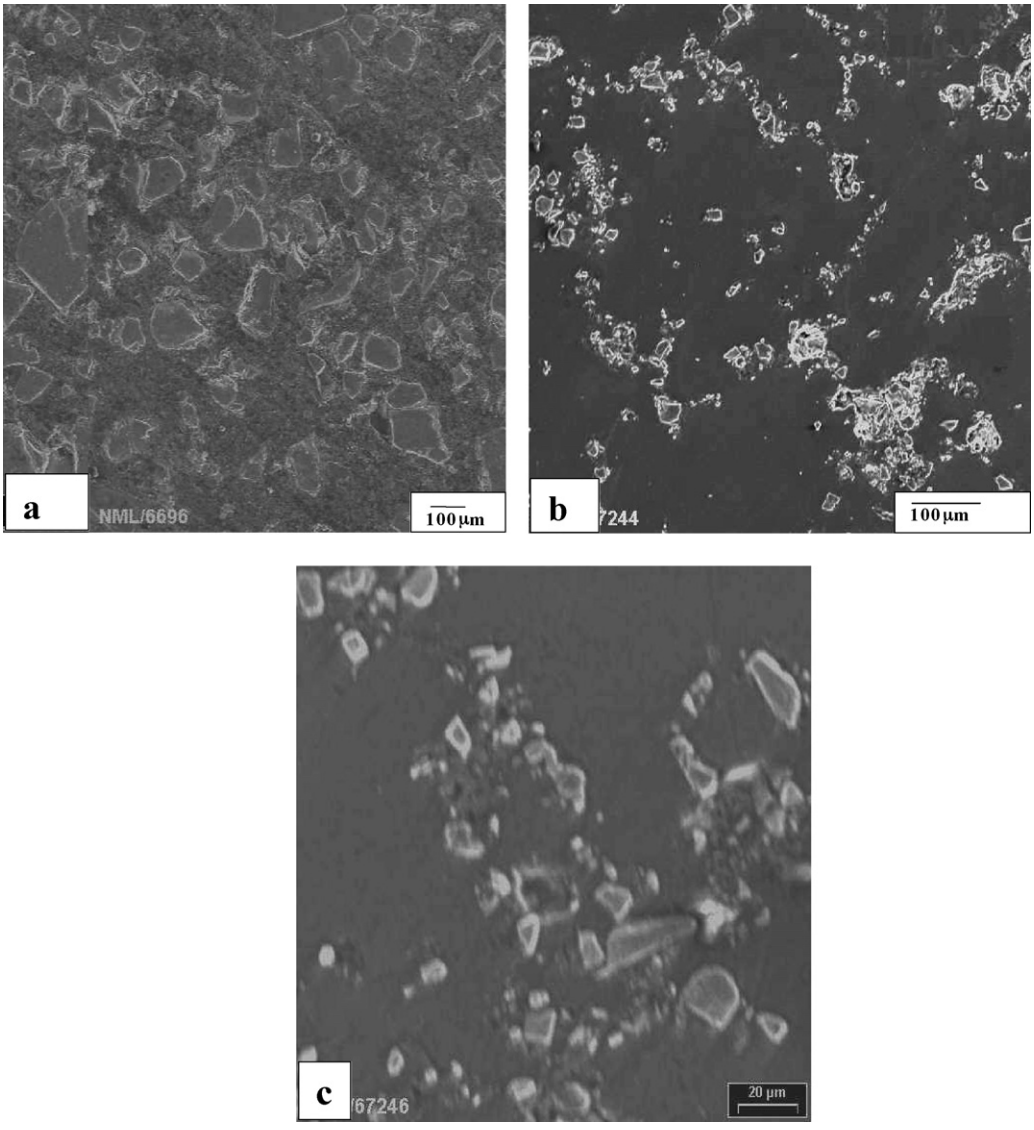

Fig. 3. SEM image illustrating microstructure of the composites: (a) C1 and (b and c) C5. All the micrographs are showing the dispersion of angular SiC particles in the respective matrices.

and 59% decrease in grain size was observed in case of C4 and C5 composites, respectively, when compared with 167 μm for A3 alloy. The AZ91D alloy (A2) shows finer grain size than the elemental Mg (A1).

Composite samples show higher hardness than that of their unreinforced counterparts (Table 4). The composite C3 with 15 μm size particles shows higher matrix hardness value than that of the composite C2 with 150 μm size particles. The microhardness near the particle/matrix interface is higher than that of interior region of the matrix in all the cases. The interfacial region in C2 and C3 composites shows considerable decrease in the hardness after T4 treatment. The tensile properties of T4 treated alloy and composites are given in Table 5. These values are an average of 5 tests. The C4 composite shows 60% higher yield strength (YS) and 8% less ultimate tensile strength (UTS) than the A3 alloy (YS = 76 MPa, UTS = 212 MPa). Similarly, composite C5 (YS = 134 MPa, UTS = 204 MPa) shows 76% increase in YS and 3.8% decrease in UTS when compared with the A3 alloy. A significant improvement of 26% and 44% in elastic modulus have been observed for C4 and C5 composites, respectively, over the A3 alloy. However, the total elongation of the above composites is drastically decreased to

Table 4
Results of hardness measurement of as cast and T4 heat-treated specimens

Material	Microhardness, HV (50 g)		Macrohardness, HV (2.5 kg) (±2 HV)
	Matrix	SiC/matrix interface	
A1	51.4 ± 0.5	–	44.9
C1	80.6 ± 0.6	113.6 ± 6	90.3
A2	77.0 ± 0.9	–	65.7
C2	81.4 ± 1.1	139.4 ± 4	91.2
C3	86.6 ± 1.5	117.1 ± 3	100.6
A3	78.1 ± 1.0	–	66.4
C4	82.2 ± 1.2	104.2 ± 2	97.5
C5	87.3 ± 1.1	102.3 ± 3	100.5

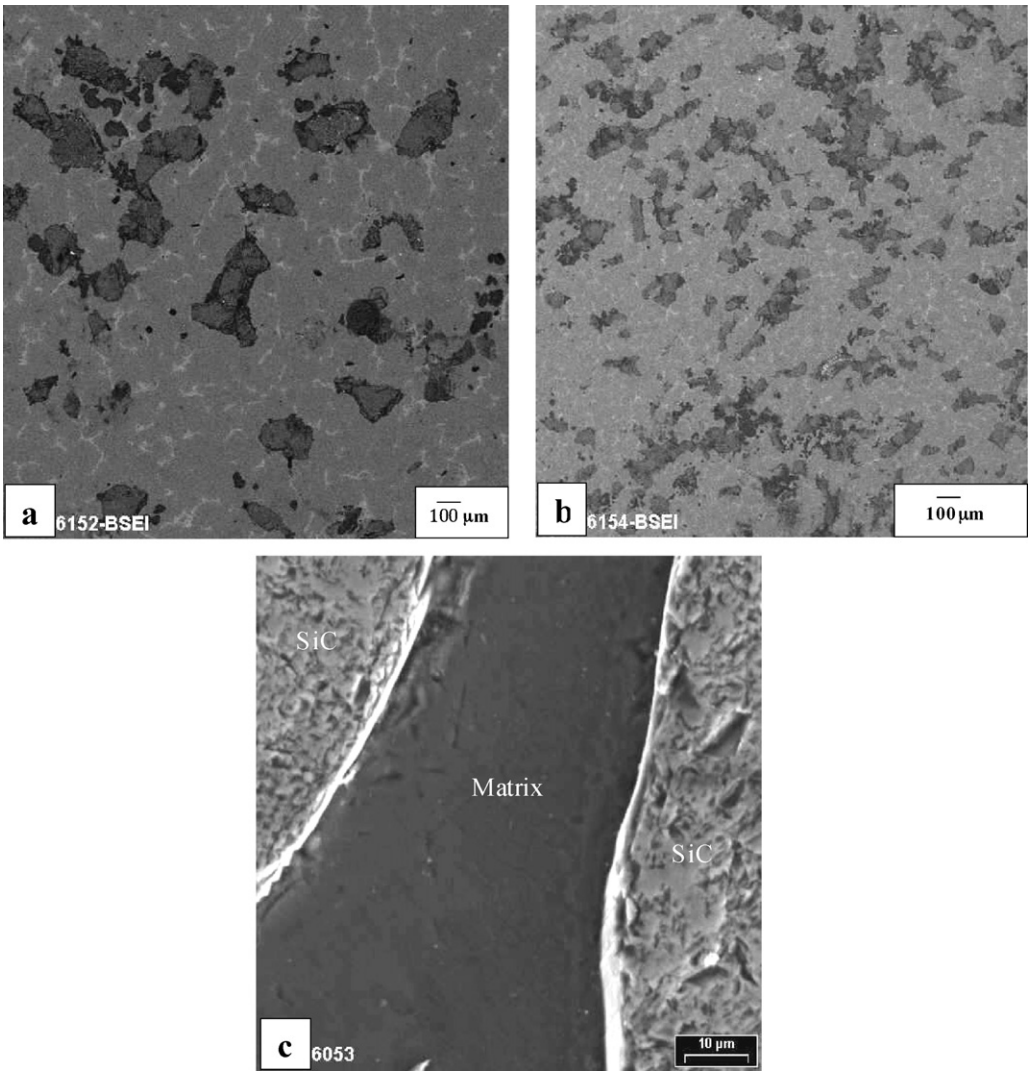

Fig. 4. SEM image of (a and b) C2 composite showing distribution of SiC particulate in A2 alloy matrix and (c) C4 composite showing the enlarged view of SiC particles almost perfectly embedded inside the A3 alloy matrix without any interface debonding.

Table 5
Tensile properties of unreinforced AZ91D alloy and composites after T4 heat-treatment

Material composition (wt.%)	0.2% yield strength (MPa)	Tensile strength (MPa)	Elongation (%)	Elastic modulus (GPa)
A3	76 ± 2	212 ± 2	7.5 ± 0.5	38.8
C4	122 ± 3	195 ± 2	0.9 ± 0.1	48.8
C5	134 ± 2	204 ± 3	1.2 ± 0.1	55.8

0.9% and 1.2% from the value of 7.6% for the unreinforced alloy.

The fracture surfaces of A3, C4 and C5 specimens are shown in Figs. 5 and 6. The fracture surface of A3 alloy (Fig. 5) reveals non-uniform ductile dimples indicating a ductile mode of fracture. Whereas, composite materials revealed a mixed mode of fracture behaviour exhibiting matrix deformation, SiC–matrix debonding and SiC particulate fracture (Fig. 6). In case of composite C4, a large number of broken SiC particles were observed in comparison with the composite C5, where few broken particles were seen. Matrix deformation and interfacial debonding coupled with microscopic cracks were observed in the fracture surface of composite C4 (Fig. 6a). In case of composite C5, matrix deformation, particle fracture (Fig. 6b) and particle pull out (Fig. 6c) were observed. This demonstrates that particle cracking is the dominant factor in the failure of composite C4, whereas particle/matrix interface debonding is dominant in the fracture process of composite C5.

4. Discussion

The synthesis of all the materials revealed low oxidation of Mg, no detectable flux/oxide inclusion, and no significant macropores. The low oxidation of Mg suggests that the exper-

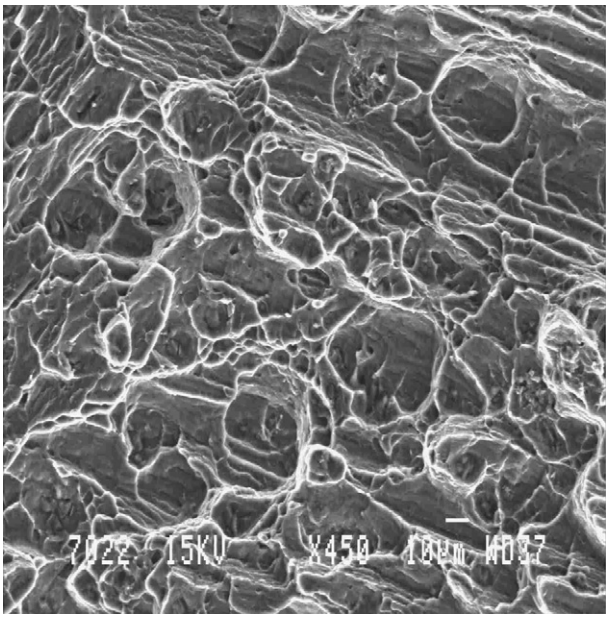

Fig. 5. SEM micrograph of the tensile fracture surface of the A3 alloy showing presence of ductile dimples of various sizes.

imental arrangements employed in the present investigation, did not permit the ingress of oxygen in the liquid metal. The successful incorporation of intended amount of 15 vol.% SiC particulates suggests that the stirring arrangement, i.e. impeller design, speed, stirring time and temperature were optimised for the incorporation of the particles. The presence of particulate agglomeration in the C3/C5 (Fig. 3b) composite may be due to finer particle size. A small size particle is more prone to clustering and also the growth of primary α-Mg grains pushes the particles towards the grain boundary. The high surface tension forces, due to large area/volume ratio at the interface and the small mass of the particles contribute to the agglomeration of particles and their clustering at the grain boundaries.

The fine-grained structure of the composite is due to the SiC addition, which leads to particle-stimulated nucleation of the primary phase. The grain refinement mechanism involving SiC addition has been well studied [10,19]. It has been reported [20] that primary Mg grain refinement results from the heterogeneous nucleation of primary Mg phase on the surface of SiC particles and the restricted grain growth by SiC particles during solidification. The particles acting as heterogeneous nucleation sites depend upon the wettability of SiC with liquid Mg. As the Mg/SiC wettability is limited, only a small number of SiC particles can act as heterogeneous nucleation sites for primary Mg, and only these SiC particles would be captured by growing Mg crystals, and finally stay within the Mg grains in the composite. This phenomena may be held responsible for the presence of particles within the grains. The limited wettability of SiC particles aids in the clustering of particles at the grain boundaries. The composite sample shows higher porosity than the unreinforced alloy. Laurent et al. [2] reported similar result in a compocast AZ91D alloy reinforced with SiC particulates. The porosity increases with decreasing particle size due to presence of interstitial voids in clusters and discontinuity caused during stirring as gas entrapment and solidification shrinkage. The SiC/matrix interfacial integrity, evaluated in terms of interfacial debonding and presence of voids, was found to be quite satisfactory. SEM observations (Fig. 4c) indicate that there is no interfacial reaction products present in the composite samples. XRD studies (Fig. 2) did not reveal any Mg_2Si-phase in the samples. This indicates that the selection of present processing temperature (700 °C maximum) is suitable for processing of these composites.

It has been observed that the macrohardness of composites are invariably higher than the monolithic alloys. This effect is attributed to the presence of hard SiC particles, which aid to the load bearing capacity of the material and also restricts the matrix deformation by constraining dislocation movement. There is not a considerable difference in the hardness of Mg and AZ91D alloy composites (C1 and C2), however, the composite containing 15 μm size particles exhibit remarkable increase in hardness even when it contains more amount of porosity. This difference is attributed to larger amount of dislocations generated due to fine size particles. The geometrically necessary dislocations increase for fine size particles compared to that for larger ones [21]. Janowski and Pletka [22] have demonstrated for Al alloy based composites that for identical dislocation density a 24 μm particle reinforcement requires only ≈8 vol.% compared to 30 vol.% for 142 μm size particle reinforcement. This can be explained as at a constant volume fraction of reinforcement, by considering the interparticle distance that decreases with decrease in particle size. This results in more inhibition sites for the movement of dislocations leading to increased hardness value. However, the result indicates that the matrix microhardness of Mg based composite is remarkably high compared to monolithic Mg. The higher dislocation density is due to the significant difference in coefficient of thermal expansion 6:1 of pure Mg and Mg-alloy with SiC particulates [23]. This indicates that the increased dislocation density in composite would have caused the increase in the hardness. Other possibility is the encounter of hard SiC particle below the indentation [21]. However, for large particle size (150 μm), this possibility could be ignored as the particle number density would be small and that hardness value is the average of several indentations. However, there is no appreciable change, both in matrix microhardness and composite macrohardness, in composites C1 and C2. This is due to the fact that in both the cases of C1 and C2, almost pure Mg grains are present. Although, the alloy in C2 has solutes but the amount of solute, with due consideration of solidification phenomena in the grain would be very less. The presence of precipitates, at the grain boundaries, in case of C2, does not affect the macrohardness values, as in this case a large number of reinforced particle interact with the indenter and contribution from the precipitates would become negligible. However, the matrix hardness near the interface is considerably high due to the fact that strained particle/matrix interface are likely places for the intermetallic precipitation. As the composite C1 does not have precipitates, the major contribution in C1 interface hardness increase, compared to the matrix, is due to the high dislocation density generated due to particle incorporation. After T4 treatment, the matrix microhardness seems to increase slightly. This may be attributed to the solution

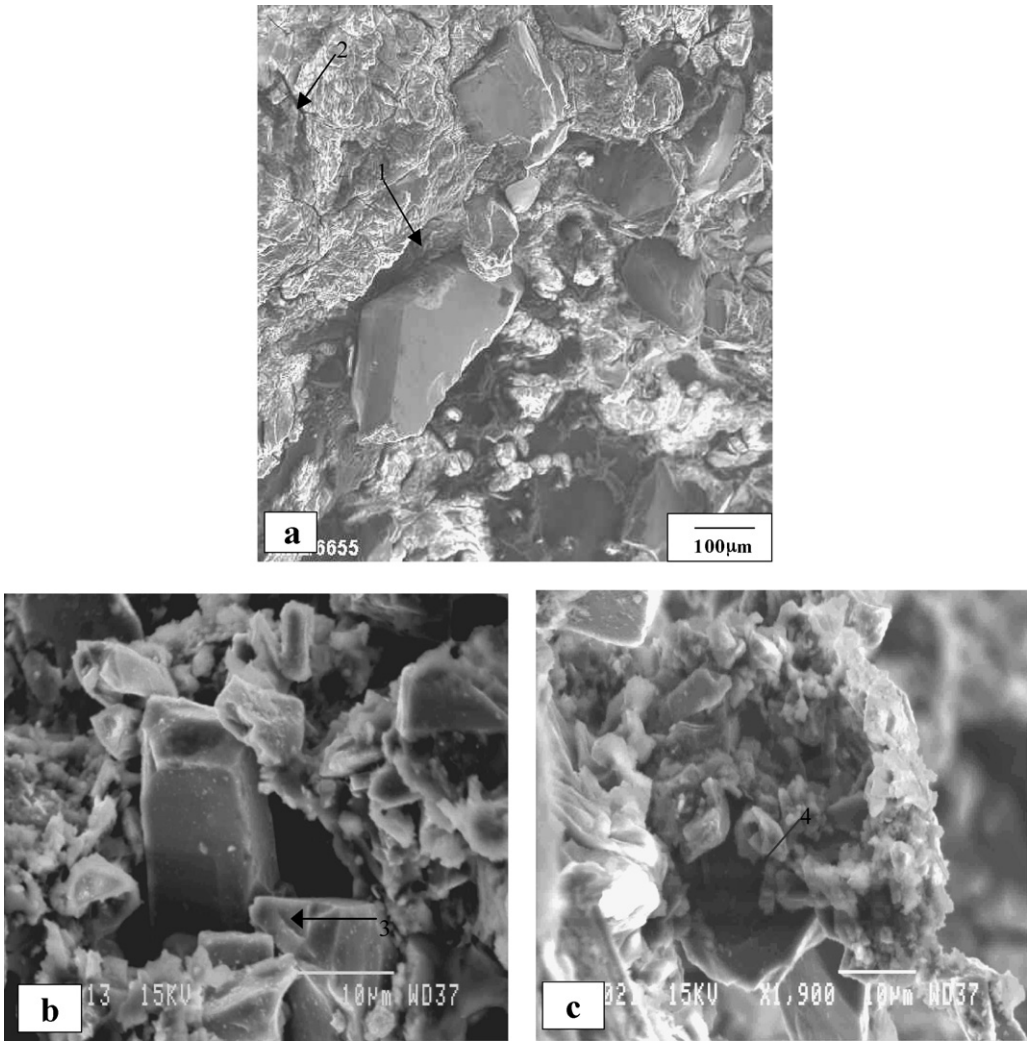

Fig. 6. SEM image of the tensile fracture surfaces: (a) C4 specimen showing interfacial debonding (arrow 1) and crack (arrow 2); (b and c) C5 specimen shows particle fracture (arrow 3) and interface debonding causing particle pull out (arrow 4).

hardening effect. The solute goes into the solution straining the lattice, which intern leads to increase in the hardness. However, the interfacial hardness decreased considerably due to the combined effect of solutionizing and relaxation of strain field around the reinforced particles. Dislocations are partially annihilated leading to decrease in hardness. However, the macrohardness of T4 treated samples are not effected considerably. However, composite C2 showed increased macrohardness after T4 treatment (C4) due to the fact that the number of particles encountered in the indentation would be less and the major effect would come from the solution hardening. Whereas, large number of small particles suppressed the effect of solution hardening for composite C5.

The tensile properties of the T4 treated alloy and composites indicated increased yield strength and elastic modulus of the composites. A smaller size reinforcement leads to better improvement in these two properties. However, the ultimate tensile strength and ductility are lower than that compared to monolithic alloy. The basic mechanism of composite deformation is the load transfer from the matrix to the reinforcement [24]. A good bonding between the matrix and the reinforced particles gives rise to better load transfer and the improved properties. This is, therefore, the imperative to avoid detrimental interfacial reaction product at the particle/matrix interface by choosing appropriate processing conditions. In a composite material, a tensile loading leads to high tensile stresses at the interface [13,25]. This may give rise to debonding at the interface or breaking of particles. In case of large deformation, voids at the interface are also seen. Failure of the composite material may take place in two ways, either by debonding or breaking of particle and crack propagation [26]. A poorly bonded interface gives way to debonding and subsequent crack growth in the matrix. Whereas, a good bond leads to failure of ceramic particles. The high elastic modulus and strength of the composite with 15 μm size particulates are attributed to the interparticle spacing. Large particle size leads to larger interparticle distance compared to small particle reinforcement. The restricted matrix flow in the small size interparticle region in composites with 15 μm size particles renders high load bearing capacity to the composite compared to the large size particle reinforced composites [27]. This exactly what leads to high elastic modulus of composite with 15 μm size particles. A large interparticle dis-

tance may give rise to large plastic deformation at the matrix phase generating voids at the particle/matrix interface. A good interfacial integrity achieved in the present investigation did not give way to void formation, particularly in the composite with smaller particle size reinforcement.

The fracture surface of A3 alloy (Fig. 5) revealed a wide size range of ductile dimples and channels formed by linear coalescence of voids. In the case of C4 and C5 specimens, evidence of areas of reasonable plastic deformation was observed and this is indicative of strain accumulation at the SiC–matrix interface (Fig. 6). The presence of SiC particle fracture and interfacial debonding was observed under SEM (Fig. 6). Such localised damage occurs when the local superposition of the internal and applied stresses becomes sufficiently high [28]. The coalescence of the localised damage at even higher strain levels then leads to the final fracture of the composite material. In case of C4 specimen, a large number of broken particles were observed as compared to C5 specimen. Composite C4 revealed less number of interfacially debonded particles when compared with the C5 composite specimen. As the particle size decreases, the dimple size decreases as a result of decreased interparticle spacing and the fracture mode changes from particle breakage to the interfacial debonding. This may be due to higher probability of having defects in coarse particles compared to that in the case of finer particles [27].

5. Conclusions

(1) A stir casting process with a melt holding and stirring at a temperature of 680 °C can be successfully utilised to synthesise reinforced magnesium based metal matrix composites with minimal porosity. The uniform distribution of SiC particulates and good SiC–matrix interface bonding indicates the suitability of present processing methodology.
(2) The presence of SiC particulate leads to significant improvement in hardness, elastic modulus and yield strength, and decrease in ultimate tensile strength and ductility. The yield strength is increased by 9.8% in the case of composite with 15 μm particle size as compared that containing 150 μm particle.
(3) The microhardness values at the region near matrix–particle interface reduced significantly after T4 treatment.
(4) A significant grain refinement is achieved due to the presence of SiC particulates in the composite material. The presence of finer reinforcement particles have greater influence on grain refinement.
(5) The unreinforced AZ91D alloy exhibits ductile type of fracture, whereas the fracture surfaces of composites show particulate breakage and SiC–matrix debonding.

Acknowledgements

The authors gratefully acknowledge the help and encouragement of Mr. Swapan Das, Mr. A. Das, Dr. G. Das, Dr. Sukomal Ghosh and Prof. S.P. Mehrotra of National Metallurgical Laboratory, during the present work.

References

[1] Magnesium Die Casting Handbook, NADACA, 1998.
[2] V. Laurent, P. Jarry, G. Regazzoni, D. Apelian, J. Mater. Sci. 27 (1992) 4447–4459.
[3] A. Martin, J. Llorca, Mater. Sci. Eng. A 201 (1995) 77–87.
[4] R.A. Saravanan, M.K. Surappa, Mater. Sci. Eng. A 276 (2000) 108–116.
[5] S.C. Sharma, B. Anand, M. Krishna, Wear 241 (2000) 33–40.
[6] C. Mayencourt, R. Schaller, Mater. Sci. Eng. A 325 (2002) 286–291.
[7] A. Luo, M.O. S Pekguleryuz, Proceedings of the 51st Annual World Magnesium Conference, International Magnesium Association, Mclean, VA, USA, 17–19 May, 1994, pp. 74–81.
[8] J.F. King, T.E. Wilks, Proceedings of the 51st Annual World Magnesium Conference, International Magnesium Association, Mclean, VA, USA, 17–19 May, 1994, pp. 26–31.
[9] A. Bochenek, K.N. Bbraszezynska, Mater. Sci. Eng. A 290 (2000) 122–127.
[10] Y. Cai, M.J. Jan, G.J. Shen, H.Q. Su, Mater. Sci. Eng. A 282 (2000) 232–239.
[11] H. Hu, Scripta Metall. Mater. 39 (1998) 1015–1022.
[12] T. Imai, S.W. Lim, D. Jiang, Y. Nishida, T. Imura, Mater. Sci. Forum 304–306 (1999) 315–320.
[13] A. Luo, Metall. Mater. Trans. A 26 (1995) 2445–2455.
[14] H. Ferkel, B.L. Mordike, Mater. Sci. Eng. A 298 (2001) 193–199.
[15] B.W. Chua, L. Lu, M.O. Lai, Compos. Struct. 47 (1999) 595–601.
[16] T. Ebert, F. Moll, K.U. Kainer, Powder Metall. 40 (1997) 126.
[17] M. Gupta, S. Ling, Mater. Des. 18 (1997) 139–147.
[18] M. Gupta, C. Lane, E.J. Lavernia, Scripta Metall. Mater. 26 (1992) 825–830.
[19] Y. Cai, D. Taplin, M.J. Tan, W. Zhou, Scripta Mater. 41 (1999) 967–971.
[20] M.C. Gui, J.M. Han, P.Y. Li, Mater. Sci. Technol. 20 (2004) 765–771.
[21] V.C. Srivastava, A. Schneider, V. Uhlenwinkel, K. Bauchkhage, Mater. Sci. Eng. A 412 (2005) 19–26.
[22] G.M. Janowski, B.J. Pletka, Metall. Mater. Trans. 26A (1995) 3027–3035.
[23] D.J. Lloyd, Int. Mater. Rev. 39 (1994) 1–23.
[24] M.C. Gui, J.M. Han, P.Y. Li, Mater. Eng. Perform. 12 (2003) 128–134.
[25] M. Manoharan, M. Gupta, M.O. Lai, D. Saravanaranganathan, Mater. Sci. Technol. 16 (2000) 670–674.
[26] P.M. Singh, J.J. Lewandowki, Metall. Trans. 24A (1993) 2531–2543.
[27] V.V. Bhanuprasad, M.A. Staley, P. Ramakrishnan, Y.R. Mahajan, Key Eng. Mater. 104–107 (1995) 495–506.
[28] Z. Wang, R.J. Zhang, Metall. Trans. A 22 (1991) 1585–1593.